Prediction of ferroelectricity in $BaTiO_3/SrTiO_3$ superlattices with domains

Y. L. Li[a)]
Department of Materials Science and Engineering, The Pennsylvania State University, University Park, Pennsylvania 16802, USA
and MPA-STC, Los Alamos National Laboratory, Los Alamos, New Mexico 87545, USA

S. Y. Hu
MST-8, Los Alamos National Laboratory, Los Alamos, New Mexico 87545, USA

D. Tenne
Department of Physics, Boise State University, 1910 University Drive, Boise, Idaho 83725, USA

A. Soukiassian and D. G. Schlom
Department of Materials Science and Engineering, The Pennsylvania State University, University Park, Pennsylvania 16802, USA

X. X. Xi
Department of Materials Science and Engineering, The Pennsylvania State University, University Park, Pennsylvania 16802, USA
and Department of Physics, The Pennsylvania State University, University Park, Pennsylvania 16802, USA

K. J. Choi and C. B. Eom
Department of Materials Science and Engineering, University of Wisconsin, Madison, Wisconsin 53706, USA

A. Saxena and T. Lookman
T-11, Los Alamos National Laboratory, Los Alamos, New Mexico 87545, USA

Q. X. Jia
MPA-STC, Los Alamos National Laboratory, Los Alamos, New Mexico 87545, USA

L. Q. Chen
Department of Materials Science and Engineering, The Pennsylvania State University, University Park, Pennsylvania 16802, USA

(Received 25 May 2007; accepted 27 August 2007; published online 14 September 2007)

The phase transitions of superlattices into single- and multidomain states were studied using a mesoscale phase-field model incorporating structural inhomogeneity, micromechanics, and electrostatics. While the predictions of transition temperatures of $BaTiO_3/SrTiO_3$ superlattices into multidomains show remarkably good, quantitative agreement with ultraviolet Raman spectroscopic and variable-temperature x-ray diffraction measurements, the single-domain assumption breaks down for superlattices in which the nonferroelectric layer thickness exceeds the characteristic domain size in the ferroelectric layers. © *2007 American Institute of Physics*.
[DOI: 10.1063/1.2785121]

Superlattices represent a fascinating class of artificially grown thin films whose atomic structures can be precisely controlled using an epitaxial technique.[1] Studies of ferroelectric/paraelectric superlattices such as $KNbO_3/KTaO_3$,[2,3] $PbTiO_3/SrTiO_3$,[4] and $BaTiO_3/SrTiO_3$ (Refs. 5–12) have revealed that the transition temperatures (T_c's) and ferroelectricity of a superlattice are strongly correlated to its structural periodicity, electrostatic interactions, and substrate strain.[13] It has also been shown that interface contributions and the domain formation may affect the dependence of transition temperatures on superlattice structural periodicity.[14] However, prior theories and atomistic calculations of superlattices have often been limited to transitions of a paraelectric superlattice to single domains within each layer of a superlattice or to a specific regular two-dimensional domain structure. In this letter, we present a theoretical model that incorporates the elastic interactions, substrate strain, electrostatic interactions, as well as three-dimensional multidomains without assuming the domain morphologies *a priori*.

As an example, we consider $(BaTiO_3)_n/(SrTiO_3)_m$ superlattices, where n and m represent the number of perovskite unit cells along the growth direction of ferroelectric $(001)_p$ oriented $BaTiO_3$ (BT) and nonferroelectric $(001)_p$ oriented $SrTiO_3$ (ST), respectively, where the subscript p denotes the pseudocubic unit cell. Our theoretical description is based on the phase-field method[15] coupled with microelasticity and electrostatics. Despite its continuum nature, such an approach has been shown to provide accurate predictions of the strain effect on T_c and domain structures of ferroelectric thin films.[16,17] In this approach, the ferroelectric domain structure is described by the polarization distribution $\mathbf{P}(\mathbf{x}) = [P_1(\mathbf{x}), P_2(\mathbf{x}), P_3(\mathbf{x})]$, where $\mathbf{x}=(x_1, x_2, x_3)$.

The total free energy of a superlattice includes the bulk free energy, elastic energy, electrostatic energy, as well as the gradient energy, i.e., $F=\int_V [f_{\text{bulk}}(P_i)+f_{\text{elas}}(P_i, \varepsilon_{ij}) + f_{\text{elec}}(P_i, E_i)+f_{\text{grad}}(P_{i,j})]dV$, where V is the volume of the superlattice film and $P_{i,j}=\partial P_i/\partial x_j$. The polarization distribution for a given temperature and time is then obtained by

[a)]Electronic mail: yulan@lanl.gov

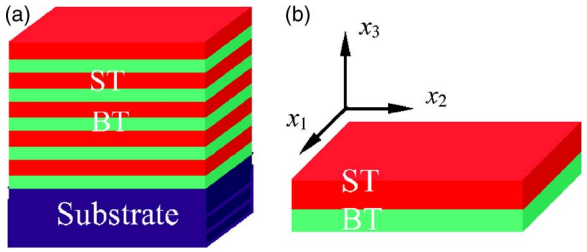

FIG. 1. (Color online) Schematic structures of (a) an epitaxial BT_n/ST_m superlattice on a substrate and (b) the simulation cell.

solving the time-dependent Ginzburg-Landau (TDGL) equations,

$$\frac{\partial P_i(\mathbf{x},t)}{\partial t} = -L\frac{\delta F}{\delta P_i(\mathbf{x},t)} \quad (i=1,2,3), \tag{1}$$

where L is the kinetic coefficient related to the domain wall mobility.

Figure 1(a) shows a schematic epitaxial superlattice consisting of periodically alternating $(001)_p$ ST and $(001)_p$ BT layers commensurately strained to the underlying $(001)_p$ ST substrate. As the film thickness of a superlattice is typically on the order of hundreds of nanometers or less, i.e., very thin compared to both the in-plane dimensions and the underlying substrate thickness, the strain arising from the substrate constraint is uniform and in plane. In the out-of-plane direction (x_3), we assume that the top surface and the film/substrate interface are charge compensated. With these assumptions, we model the superlattice as a periodic structure, as shown in Fig. 1(b).

The bulk free energy $[f_{\text{bulk}}(P_i)]$ is expanded into the Landau polynomial in terms of the polarization components.[18] The corresponding nonzero coefficients can be found in Refs. 18 and 19, as well as the lattice parameters and the elastic and electrostrictive properties of cubic/pseudocubic ST and BT single crystals used in the following calculations. The variation of the coefficients and properties within the superlattice is described by a phase-field variable $\phi(x_3)$, i.e., $\zeta=\zeta_{\text{ST}}+\phi(x_3)(\zeta_{\text{BT}}-\zeta_{\text{ST}})$, where $\phi(x_3)$ represents a given property and takes the values of 1.0 in BT and 0.0 in ST. Across the BT/ST interface, we assume that the properties change linearly over the interfacial thickness.

The elastic energy density is obtained using the usual linear elasticity, $f_{\text{elas}}=(1/2)c_{ijkl}(\mathbf{x})[\varepsilon_{ij}(\mathbf{x})-\varepsilon^0_{ij}(\mathbf{x})][\varepsilon_{kl}(\mathbf{x})-\varepsilon^0_{kl}(\mathbf{x})]$, where $c_{ijkl}(\mathbf{x})$ is the elastic stiffness tensor, $\varepsilon_{ij}(\mathbf{x})$ is the total strain, and $\varepsilon^0_{ij}(\mathbf{x})$ is the stress-free strain. The summation convention for repeated indices is implied with $i, j, k, l=1,2,3$. Both ε_{ij} and ε^0_{ij} are defined with respect to the cubic ST substrate as the reference. The stress-free strain ε^0_{ij} consists of two contributions: the ferroelectric transition and the lattice mismatch with respect to the substrate, i.e., $\varepsilon^0_{ij}(\mathbf{x})=Q_{ijkl}(\mathbf{x})P_k(\mathbf{x})P_l(\mathbf{x})+\varepsilon^{\text{latt}}_{ij}(\mathbf{x})$, where $Q_{ijkl}(\mathbf{x})$ represents the electrostrictive coefficients. The elastic solution was obtained using the microelasticity theory[20] of Khachaturyan and Shatalov together with an iterative method.[21] The electrostatic energy in the superlattice is given by $f_{\text{elec}}=-(1/2)E_iP_i$. As $E_i=-\varphi_{,i}$, the electrostatic equilibrium equation is expressed as $\omega_0\varphi_{,ii}=P_{i,i}$, where ω_0 is the dielectric permittivity of vacuum. The gradient energy is the energy penalty for the spatial variation of the polarization field and can be expressed as $f_{\text{grad}}=(1/2)g_{ijkl}(\partial P_i/\partial x_j)(\partial P_k/\partial x_l)$, where g_{ijkl} is the gradient energy coefficient.

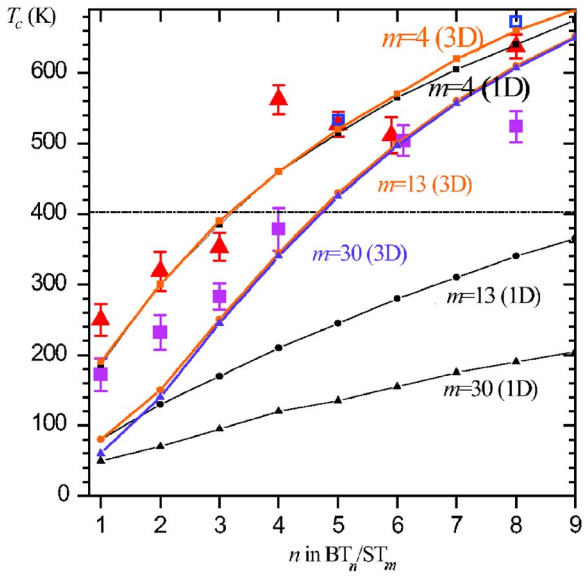

FIG. 2. (Color online) Dependence of T_c on n and m in commensurate BT_n/ST_m superlattices on (001) ST substrates. The symbols connected by lines are from the phase-field calculations with multidomain (3D) and single-domain (1D) states, respectively. The scattered solid squares ($m=13$) and triangles ($m=4$) are from UV Raman spectroscopic measurements, and the open squares are from VTXRD measurements ($m=4$).

We employed a simulation cell of $(64\Delta x_1)(64\Delta x_2)\times(N\Delta x_3)$, where $N=2(n+m)$ for a BT_n/ST_m superlattice. A grid spacing of $\Delta x_1=\Delta x_2=1.0$ nm and $\Delta x_3=0.5a_{\text{ST}}$ was used. The gradient energy coefficient was assumed to be isotropic with the nonzero independent one $g_{1111}/g_0=2.0$. g_0 is related to Δx_1 by $\Delta x_1=\sqrt{g_0/\alpha_0}$ and $\alpha_0=|\alpha_{1\text{BT}}|_{T=298\text{ K}}$. The width of the BT/ST interface is assumed to be one grid spacing Δx_3. Starting from a small random polarization distribution, we solved the coupled elastic, electrostatic, and the TDGL equations to obtain the domain morphologies. We identify the temperature below which there exists a spontaneous polarization as T_c.

Figure 2 summarizes the predicted T_c as a function of BT and ST layer thicknesses for phase transitions into either a single domain (labeled 1D) with $\mathbf{P}=\mathbf{P}(x_3)$ or multidomain (labeled 3D) state with $\mathbf{P}=\mathbf{P}(x_1,x_2,x_3)$ as well as T_c values determined from UV Raman and variable-temperature x-ray diffraction (VTXRD) measurements.[12] As expected, T_c increases with the number of unit cells n of ferroelectric BT layers and decreases with the number of nonferroelectric ST unit cells m. While the difference in T_c between transitions to single-domain and multidomain states is small for ST layer thickness $m=4$, for larger $m(=13,30)$, the predicted T_c's for transitions to single-domain states are significantly lower than those to multidomain states. Furthermore, based on the multidomain results, superlattices with $m=13$ and 30 have very similar T_c values, implying that T_c no longer changes with m for large m, and the effect of the ST layer thickness on T_c diminishes as the thickness of the BT layer n increases. Finally, the predicted T_c's for transitions to multidomain states and experimentally measured values show very good quantitative agreement.

To understand the difference between transitions to single-domain and multidomain states, we examined the polarization distribution and domain morphologies. An example of a domain morphology from a 3D simulation is shown in Fig. 3(a) for a BT_8/ST_{13} superlattice at a tempera-

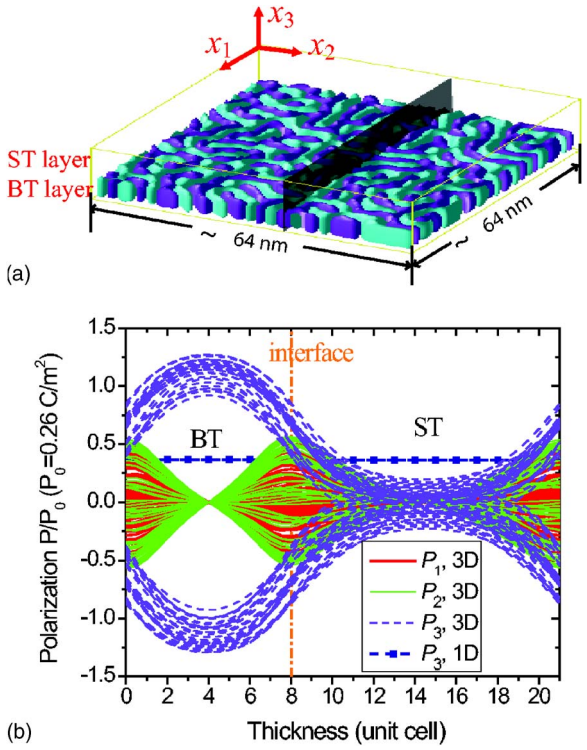

FIG. 3. (Color online) (a) Domain morphology of a BT_8/ST_{13} superlattice. The two colors in the BT layer indicate domains with up and down polarizations, respectively. (b) Projections of the polarization components (P_1, P_2, P_3) in the cross section shown in gray in (a) onto a line along x_3 at $x_1=0$.

ture of $T=300$ K. There are two types of domains (represented by two different colors) with opposite, out-of-plane polarization directions, i.e., tetragonal c domains separated by 180° domain walls within the BT layer. The magnitude of polarization in the ST layer [represented by empty part in Fig. 3(a)] is significantly less. The projections of the three polarization components at a particular x_2 value indicated by the gray plane in Fig. 3(a) onto a line along x_3 at $x_1=0$ are plotted in Fig. 3(b). The out-of-plane component P_3 has its maximum at the middle of the BT layer, decreases gradually from the BT layer to the ST layer, and is close to zero in the middle of the ST layer. The in-plane components P_1 and P_2 are not absolutely zero. In fact, they have small values around the 180° domain walls and are maximal around the ST/BT interfaces. This means that across the 180° domain walls, the polarization switches its direction continuously. This cannot be seen if we assume that $\mathbf{P}=\mathbf{P}(x_3)$, the 1D model.

For phase transitions to a single domain of $\mathbf{P}=\mathbf{P}(x_3)$, a large polarization [the squares connected by a line in Fig. 3(b)] appears in the unstrained ST layers, which is slightly lower than the polarization in the surrounding BT layers. This differs dramatically from the polarization distributions of a multidomain state of $\mathbf{P}=\mathbf{P}(x_1,x_2,x_3)$, but is in agreement with recent first-principles calculations (which assume a single domain) of short-period BT_n/ST_m $(n+m=5)$ superlattices.[6] Our simulations show that the polarization in the ST disappears when the dipole-dipole interaction is artificially switched off. Therefore, the polarization within the ST is not the result of a ferroelectric phase transition, rather it is induced by the dipolar field produced by the BT layer, i.e., a result of a "ferroelectric proximity" effect. The induced polarization in the ST layer and thus the depolarization field can be significantly reduced or almost eliminated by the formation of domains within the BT layers. On other hand, our simulations demonstrated that the effect of domains on T_c can be neglected only if the thickness of the nonferroelectric layer is much smaller than the characteristic domain size within the ferroelectric layer, which are on the order of a couple of nanometers (~3–4 nm in our particular example of BT_n/ST_m superlattices).

In summary, we developed a phase-field model for predicting the phase transitions and ferroelectricity of superlattices. In particular, we studied the roles of multidomain states in phase transitions of superlattices. The predicted T_c's of ST/BT superlattices to multidomain states are in excellent agreement with experimental measurements, while the single-domain assumption breaks down at large layer thickness of the nonferroelectric layer, revealing the importance of domain formation in determining phase transition temperatures and other important aspects of ferroelectricity in superlattices.

This work was partially supported by Los Alamos National Laboratory Directed Research and Development Project under the United States Department of Energy (DOE), by NSF under DMR-0213623, DMR-0507146, and ECS-0210449, and by DOE under DE-FG02-01ER45907.

[1] D. G. Schlom, J. H. Haeni, J. Lettieri, C. D. Theis, W. Tian, J. C. Jiang, and X. Q. Pan, Mater. Sci. Eng., B **87**, 282 (2001).
[2] E. D. Specht, H. M. Christen, D. P. Norton, and L. A. Boatner, Phys. Rev. Lett. **80**, 4317 (1998).
[3] M. Sepliarsky, S. R. Phillpot, D. Wolf, M. G. Stachiotti, and R. L. Migoni, J. Appl. Phys. **90**, 4509 (2001).
[4] M. Dawber, C. Lichtensteiger, M. Cantoni, M. Veithen, P. Ghosez, K. Johnston, K. M. Rabe, and J. M. Triscone, Phys. Rev. Lett. **95**, 177601 (2005).
[5] H. Tabata, H. Tanaka, and T. Kawai, Appl. Phys. Lett. **65**, 1970 (1994).
[6] J. B. Neaton and K. M. Rabe, Appl. Phys. Lett. **82**, 1586 (2003).
[7] K. Johnston, X. Y. Huang, J. B. Neaton, and K. M. Rabe, Phys. Rev. B **71**, 100103 (2005).
[8] L. Kim, J. Kim, D. Jung, J. Lee, and U. V. Waghmare, Appl. Phys. Lett. **87**, 052903 (2005).
[9] W. Tian, J. C. Jiang, X. Q. Pan, J. H. Haeni, Y. L. Li, L. Q. Chen, D. G. Schlom, J. B. Neaton, K. M. Rabe, and Q. X. Jia, Appl. Phys. Lett. **89**, 092905 (2006).
[10] S. Rios, A. Ruediger, A. Q. Jiang, J. F. Scott, H. Lu, and Z. Chen, J. Phys.: Condens. Matter **15**, L305 (2003).
[11] A. Q. Jiang, J. F. Scott, H. B. Lu, and Z. H. Chen, J. Appl. Phys. **93**, 1180 (2003).
[12] D. A. Tenne, A. Bruchhausen, N. D. Lanzillotti-Kimura, A. Fainstein, R. S. Katiyar, A. Cantarero, A. Soukiassian, V. Vaithyanathan, J. H. Haeni, W. Tian, D. G. Schlom, K. J. Choi, D. M. Kim, C.-B. Eom, H. P. Sun, X. Q. Pan, Y. L. Li, L. Q. Chen, Q. X. Jia, S. M. Nakhmanson, K. M. Rabe, and X. X. Xi, Science **313**, 1614 (2006).
[13] S. Zhong, S. P. Alpay, A. L. Roytburd, and J. V. Mantese, IEEE Trans. Ultrason. Ferroelectr. Freq. Control **53**, 2349 (2006).
[14] V. A. Stephanovich, I. A. Luk'yanchuk, and M. G. Karkut, Phys. Rev. Lett. **94**, 047601 (2005).
[15] L. Q. Chen, Annu. Rev. Mater. Res. **32**, 113 (2002).
[16] Y. L. Li, S. Y. Hu, Z. K. Liu, and L. Q. Chen, Appl. Phys. Lett. **78**, 3878 (2001).
[17] Y. L. Li, S. Y. Hu, Z. K. Liu, and L. Q. Chen, Acta Mater. **50**, 395 (2002).
[18] Y. L. Li, L. E. Cross, and L. Q. Chen, J. Appl. Phys. **98**, 064101 (2005).
[19] BT: $c_{11}=1.78\times10^{11}$, $c_{12}=0.964\times10^{11}$, $c_{44}=1.22\times10^{11}$, $Q_{11}=0.10$, $Q_{12}=-0.034$, $Q_{44}=0.029$; $a=3.9994\times10^{-10}+5.353\,86\times10^{-15}(T-273)$; ST: $\alpha_1=2.6353\,[\coth(42/T)-0.90476]\times10^7$, $\alpha_{11}=1.696\times10^9$, $\alpha_{12}=1.373\times10^9$, $c_{11}=3.36\times10^{11}$, $c_{12}=1.07\times10^{11}$, $c_{44}=1.27\times10^{11}$, $Q_{11}=0.066$, $Q_{12}=-0.0135$, $Q_{44}=0.0096$; $a=3.9043\times10^{-10}[(1+9.39)\times10^{-6}(T-273)+1.97\times10^{-9}(T-273)^2]$, where a is the pseudocubic lattice parameter, c_{ij} and Q_{ij} are the Voigt notation for c_{ijkl} and Q_{ijkl} (in SI units and T in kelvin).
[20] A. G. Khachaturyan and G. A. Shatalov, Sov. Phys. JETP **29**, 557 (1969).
[21] S. Y. Hu and L. Q. Chen, Acta Mater. **49**, 1879 (2001).